

Contents list available at CBIORE journal website

RE International Journal of Renewable Energy Development

Journal homepage: https://ijred.cbiore.id



Research Article

Numerical simulation of co-firing oil palm fronds and lignite coal injected at different burning rates in tangential pulverized coal burner

Sobar Ihsan^{a,b}, Prabowo Prabowo^a, Wawan Aries Widodo^a, I Nyoman Agus Adi Saputra^a

Abstract. Reducing CO₂ emissions and utilizing biomass, particularly palm oil mill waste, is crucial for addressing climate change, enhancing air quality, and advancing environmentally sustainable clean technology innovations. *Palm fronds* can serve as a renewable fuel source with minimal emissions, providing a viable co-firing option for coal in coal-fired power plants (PLTU). Although previous studies have shown promising *CO*₂ emission reductions through co-combustion of oil palm fronds and coal, there is still no comprehensive analysis of the combustion characteristics and emission behavior when varying the burner injection zone, thus further research is required. This study performs a numerical analysis using three-dimensional *computational-fluid dynamics* (CFD) to examine the co-burning process of *palm fronds* alongside *low-calorie coal* (LRC) at the Pacitan PLTU, which has a capacity of 315 megawatts. The co-burning simulation, incorporating a 5% substitution of *palm fronds* in each burner, was conducted to differentiate between burners A and D, aiming to determine the optimum injection area. The findings of the simulation reveal inconsistencies in combustion properties, particularly regarding temperature allocation. The primary results demonstrate a temperature rise when palm fronds are used as a co-firing fuel, attributed to their greater volatility and oxygen content compared to coal. The most notable decrease in *CO*₂ emissions was observed with the substitution of 5% *oil palm fronds* in burner B; however, the reduction was not substantial, as indicated by a mass fraction value of 0.128 at the boiler discharge. An increase in *NOx* mass fraction was also observed due to the organic nitrogen in *palm frond* biomass, which decomposes rapidly during combustion at high temperatures. This co-firing technology is expected to provide a means for lowering emissions and improving the use of alternative fuels as a substitution for fossil fuels in a time to come.

Keywords: Boiler; Computational fluid dynamics; Co-firing; Oil palm fronds; LRC



@ The author(s). Published by CBIORE. This is an open-access article under the CC BY-SA license (http://creativecommons.org/licenses/by-sa/4.0/).

Received: 27th Dec 2024; Revised: 6th March 2025; Accepted: 21st April 2025; Available online: 30th April 2025

1. Introduction

In light of global demands for net-zero emissions, researchers are examining the viability of renewable energy sources as alternatives to fossil fuels. Indonesia has diverse energy sources, particularly biomass and agricultural waste, which are critical to energy metrics. In the last few years, a remarkable increase is recorded in the extent of palm oil plantations, driven by the strong global consumption for palm oil products (Lam et al., 2015). This surge in palm oil production has resulted in substantial amounts of waste generated from plantations. It is estimable that about 90% of the entire biomass from oil palm cultivation remains underutilized, including materials such as palm kernel shells (PKS), oil palm fronds (OPF), empty fruit bunches (EFB), and palm fibers, which are often discarded as waste (Aziz, Prawisudha, et al., 2015). This situation creates difficulties related to the improper administration of palm oil waste. There is an urgent need for innovative approaches to repurpose oil palm fronds as a sustainable energy alternative, addressing both environmental and economic considerations (Cahyo et al., 2024).

A pragmatic approach to utilizing oil palm fronds in energy generation is coal co-firing, acknowledged as an economical and successful method for transforming oil palm trash into electricity. Indonesia, albeit the foremost coal producer, encounters limitations in fuel availability for electricity generation (Ihsan *et al.*, 2023). Regrettably, although Indonesia is the foremost coal producer, it encounters a limited fuel supply for electricity generating (Putra *et al.*, 2023).

Moreover, the recognition of environmental effects has prompted the general public and policymakers to adopt ecofriendly technologies and energy sources. The most effective approach to resolve these challenges and prolong the operational lifespan of power plants and coal reserves is the concurrent combustion of biomass and coal (Arifin et al., 2023). Numerous innovative approaches to enhance the properties of biomass fuels have been explored, including drying (Aziz, Oda, et al., 2015; Lucian & Fiori, 2017), hydrothermal processing (Hariana et al., 2023a; Tirumareddy et al., 2024), torrefaction (Torres Ramos et al., 2023; Z. Wang et al., 2021; Wongsiriwittaya et al., 2023), pyrolysis (Chae et al., 2021; Ghosh et al., 2023; Usino et al., 2023), pelletization (Garcia-Nunez et al., 2016; Kim et al., 2009), and carbonization (Jamari & Howse, 2012; Kumar et al., 2025). Hydrothermal (HT) processing is a technique under investigation, employed as a pre-treatment method prior to the thermo-chemical conversion of biomass. This method entails

^aMechanical Engineering Department, Institut Teknologi Sepuluh November, Indonesia

^bMechanical Engineering, University Islamic Kalimantan Muhammad Arsyad Al Banjari, Indonesia

applying water at temperatures ranging from 180°C to 250°C under high pressure 5-10 MPa (Ibbett *et al.*, 2011; Liu *et al.*, 2013). Oil palm frond biomass demonstrates superior combustion properties compared to palm kernel shell (PKS) and empty fruit bunch (EFB), substantially reducing the formation of deposits and sticky substances that contribute to fouling (Hariana *et al.*, 2023b). The optimization of particle combustion is evident, as combustion products are swiftly expelled from the boiler heat exchanger prior to entering the boiler (Agus Adi Saputra *et al.*, 2023; Su *et al.*, 2024).

Additionally, various investigations have explored the cofiring properties of palm oil waste biomass and coal in traditional power plants with no structural alterations, utilizing computational fluid dynamics (CFD). The materials like palm oil waste have been analyzed include various types, such as palm fronds (Ihsan *et al.*, 2024; Rahman *et al.*, 2023), hydrothermal empty fruit bunches (Agus Adi Saputra *et al.*, 2024; Darmawan *et al.*, 2017; Jiang *et al.*, 2020), and palm kernel shells (Aziz *et al.*, 2016). Computational fluid dynamics serves as a valuable tool for examining the thermal properties of co-firing combustion (Bhuiyan *et al.*, 2016a).

Given the robust potential of OPF as a biomass fuel and the prevalence of coal-fired power plants, particularly in Indonesia, implementing OPF in conjunction with a hydrothermal process as a co-firing material for coal-based power plants is regarded as a significant endeavor. Prior research suggests that the ideal co-firing combustion configuration for a mixture of oil palm frond biomass and coal is a 5% blending ratio. This ratio has resulted in increased combustion temperatures and improved speed distribution, while reducing CO₂ emissions (Ihsan et al., 2024). Regrettably, no research has examined the effects of cofiring HT-OPF biomass in various burner zones. Hence, the primary objective of this research is to conduct computational fluid dynamics simulations with a 5% substitution ratio to analyze combustion temperatures in the combustion chamber and investigate the emissions of CO₂, SO₂, and NOx in tangential pulverized coal boilers. This investigation aims to determine the optimal co-firing strategy for HT-OPF biomass and coal.

2. Coal Co-firing of Biomass HT-OPF

Fig. 1 illustrates a basic conceptual diagram of an HT-OPF and coal co-firing system as a source of electrical power generation. The dashed lines and solid arrows represent the material and energy flows (heat and electricity sources).

The initial step involves shredding the raw oil palm fronds into smaller pieces before subjecting them to hydrothermal

processing. Hydrothermal processes are typically conducted in water below 250 °C (Li *et al.*, 2017). Researchers have examined high-temperature use in various biomass processes to produce hydrocarbons (Chiaramonti *et al.*, 2017; Román *et al.*, 2012). To eliminate the need for a drying stage following the hot-pressing process, HT-OPF utilizes a consistently elevated temperature surpassing the saturation temperature. Consequently, the water vapour contained in the OPF is evaporated and released alongside the water vapour utilized in the heat transfer process. The HT-OPF combination is subsequently removed from the reactor using a relatively small volume of water.

Concurrently, the coal is first ground and dehydrated to a lower moisture content before being mixed with HT-OPF. The combined coal and biomass HT-OPF fuel mixture is combusted in a combustion chamber, producing high-temperature heat, which is then used to generate steam for power generation via a boiler. Subsequently, the process directs the steam into a steam turbine, which rotates a generator to produce the requisite electricity. Furthermore, the exhaust gas exiting the boiler is employed for post-HT *drying* and coal processing.

3. Numerical Modeling for Co-firing Coal and HT-OPF

3.1 Domain and Materials

The pulverized coal (PC) boiler domain illustrated in Fig. 2 showcases a currently operational coal-fired power plant with a 315 Mwe capacity. It includes a drawing of the boiler's layout down to the bottom ash, combustion region, overfire air (OFA) zone, flue gas exit temperature (FEGT) zone, burner inlet, heating section, and boiler outlet. The dimensions of the boiler are long (36,200 mm), wide (13,700 mm), and high (63,700 mm).

Figure 3 illustrates the schematic configuration of the pulverized coal boiler utilized in the co-firing simulation study. The boiler structure comprises several essential zones: the Bottom Ash Zone (BAZ), Lower Burning Zone (LBZ), Upper Burning Zone (UBZ), Overfire Air (OFA) Zone, and Flue Gas Exit Temperature (FEGT) Zone. The combustion process initiates in the lower and upper combustion zones, subsequently resulting in heat recovery in the upper parts. The heating part of the boiler is designed with numbered components to illustrate the sequence of heat absorption. 1. Panel Superheater (SH), 2. Platen Superheater (SH), 3. Medium Reheater (RH), 4. Final Reheater (RH), 5. Final Superheater (SH). After the combustion and heating zones, the flue gas traverses the following

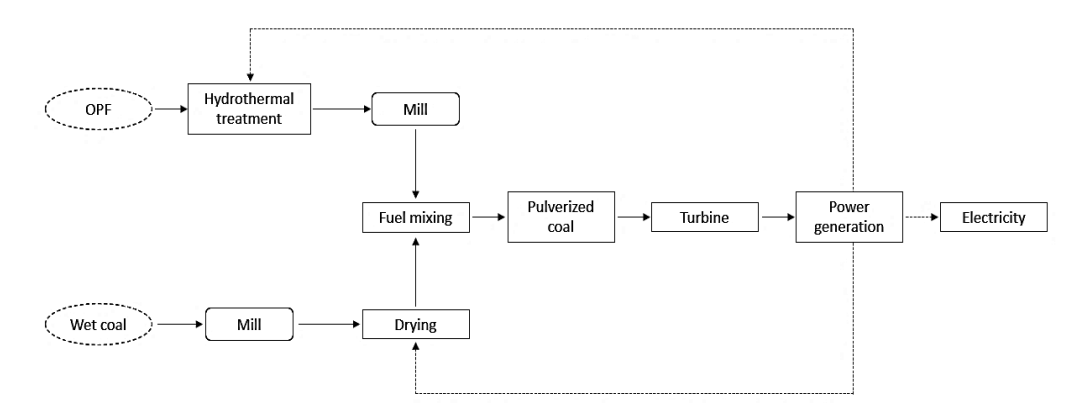


Fig. 1. Fundamental schematic representation of the HT-OPF and coal co-firing system

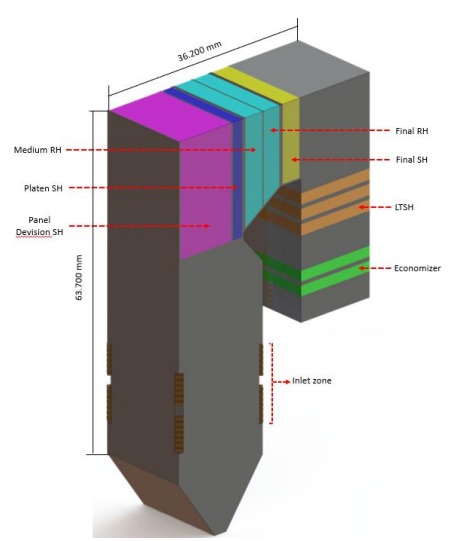


Fig. 2. Steam power plant boiler simulation

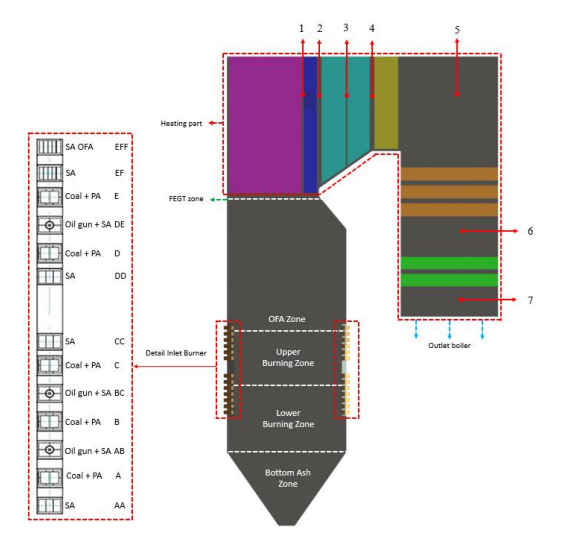


Fig. 3. Establish boundary conditions and conduct point validation of the steam power facility

Table 1Composition of materials

| Component | Coal LRC | Biomass HT-OPF |
|---------------------------|----------|----------------|
| Proximate Analysis | | |
| Volatile Matter (wt %) | 33.76 | 77.81 |
| Fixed Carbon (wt %) | 32.31 | 14.29 |
| Ash (wt %) | 2.50 | 2.09 |
| Moisture (wt %) | 31.43 | 5.81 |
| Ultimate Analysis | | |
| Carbon (wt %) | 46.96 | 44.37 |
| Nitrogen (wt %) | 0.66 | 0.46 |
| Oxygen (wt %) | 15.04 | 41.66 |
| Hydrogen (wt %) | 3.29 | 5.51 |
| Calorific Value (Kcal/kg) | 4452 | 3941 |
| Sulfur (wt %) | 0.12 | 0.10 |

components: 6. Low-Temperature Superheater (SH) and 7 Economizer section before being expelled through the outlet boiler. Each component is essential for enhancing the thermal efficiency of the steam generation process by systematically lowering the flue gas temperature and increasing the enthalpy of the working fluid. The boundary conditions, encompassing mass-flow inlets for primary and secondary air and the pressure outlet, are configured to accurately simulate actual boiler operation. The coal employed in the simulation is sourced from Kalimantan, Indonesia. LRC coal is distinguished by its low calorific value and elevated moisture content. The oil palm fronds are sourced from a palm oil facility in Sumatra, Indonesia, and undergo hydrothermal treatment. Table 1 presents the proximate and ultimate analyses of the LRC and HT-OPF coals employed in this study, outlining their composition.

3.2 Boundary Condition

Boundary conditions are categorized into four distinct types, as illustrated in Fig. 2: interior, pressure outlet, mass flow inlet, and wall. The mass-flow inlet is selected because the primary and secondary-air enter the boiler in a specific quantity, which is regulated by a constant value for the incoming airflow, to accurately reflect the real circumstances in the PLTU. The pressure outlet indicates the pressure at the end of the boiler, generally assumed to be close to atmospheric pressure or slightly lower as a result of the chimney's suction effect. A wall serves as a fixed boundary that restricts mass exchange and

Table 2Boiler parameters for case study and findings

| | Operation Boiler | | Simulatio | n Cases | |
|---|------------------|--------------------|-----------|---------|--------|
| | Case 1 | Case 2 | Case 3 | Case 4 | Case 5 |
| Combustion Type | Pure Coal | ure Coal Co-firing | | | |
| T-FRD Bleeding Ratio (%, Thermal Basis) | 0 | 5 | 5 | 5 | 5 |
| Fuel Mills (Burn Zone) | #ABCD | #A | #B | #C | #D |
| Coal Feed Rates (kg/s) | 10.61 | 10.08 | 10.08 | 10.08 | 10.08 |
| Biomass Feed Rates (kg/s) | - | 2.52 | 2.52 | 2.52 | 2.52 |
| SA ^a Flow Rate (kg/s) | 190.74 | | | | |
| OFA a Flow Rate (kg/s) | | 44 | 1.36 | | |
| PA ^a Flow Rate (kg/s) | | 97 | 7.62 | | |
| PA (K) Temperature | | 32 | 26.9 | | |
| SA (K) Temperature | | 59 | 96.6 | | |
| OFA (K) Temperature | | 59 | 96.6 | | |
| CO ₂ Reduction (%) | - | 27.96 | 28.50 | 30.72 | 31.18 |
| SO ₂ Reduction (%) | - | 18.75 | 19.10 | 19.65 | 20.05 |
| NOx Increase (%) | - | +26.76 | +28.27 | +30.34 | +32.27 |
| Temperature Increase (%) (Afterburner Zone) | - | 11.49 | 12.30 | 13.05 | 13.25 |

^a Primary Air (PA), Overfire Air (OFA), and Secondary Air (SA),

Table 3Establish point properties for coal and HT-OPF on each burner

| No. | Name | Fuel Type | LRC Ratio (%) | OPF Ratio (%) | Coal Burner | OPF Burner |
|--------|-----------------|------------|---------------|---------------|-------------|------------|
| Case 1 | 100% LRC | Coal | 100 | 0 | PA ABCD | - |
| Case 2 | 5% OPF Burner A | Coal + OPF | 95 | 5 | PA ABCD | PA A |
| Case 3 | 5% OPF Burner B | Coal + OPF | 95 | 5 | PA ABCD | PA B |
| Case 4 | 5% OPF Burner C | Coal + OPF | 95 | 5 | PA ABCD | PA C |
| Case 5 | 5% OPF Burner D | Coal + OPF | 95 | 5 | PA ABCD | PA D |

Table 4Mesh data for grid independence test

| Meshing Model | Elements | Nodes | Deviation Error % |
|---------------|----------|----------|-------------------|
| Meshing #A | 474.764 | 1956.757 | 10.04 |
| Meshing #B | 737.426 | 3007.994 | 3.8 |
| Meshing #C | 1386.233 | 5580.517 | -4.86 |

heat transfer. The primary and secondary air inlets are designated as mass flow inlets, and the boiler outlet is designated as a pressure discharge. The primary air functions as a priming gas, enabling the transport of fuel (including coal particles) via the inner pipe. The input burners #A, #B, #C, #D, and #E facilitate the introduction of the HT-OPF into the furnace. Burner #E is inoperative un this simulation; hence, it is seen as a wall. Secondary air is supplied into the furnace via intake burners #AA, #BC, #AB, #DD, #EF, #CC, #DE, and #EFF, providing the supplementary air necessary for combustion as it traverses the outer pipe.

This study employs a geometric model comprising multiple primary zones, including the bottom ash zone (BAZ), overfire air zone (OFA), and furnace exit gas temperature (FEGT), as seen in Fig. 2. The combustion chamber directly influences the airflow pattern, fuel mixing, and temperature distribution throughout the furnace. The air-fuel ratio is maintained at the same level as that of pure coal combustion conditions. Table 2 shows the details of the boiler parameters for the case study and the findings compared in various operating scenarios and simulations. The airflow ratio utilized is presented in Table 3, according to the simulation data. This combustion setup entails the injection of 5% oil palm fronds into burners #A, #B, #C, and #D, while burner #E is designated as a wall and remains inactive. Table 4 shows the mesh data used for the grid independence test, which compares three meshing models with varying resolutions. Meshing #B was selected for further simulation as it offers a good balance between computational efficiency and accuracy, with an acceptable deviation error of 3.8%. While this number has been modified to meet combustion requirements, the precise influence of fluctuations in the air-fuel ratio on thermal efficiency and exhaust gas emission characteristics can be further explored in the future.

3.3 Computational Modeling

CFD modeling represents the most effective method for calculating a range of processes, including chemical reactions, heat and mass transfer, and fluid flow (Y. Wang & Yan, 2008). Compared to experimental investigations, the CFD method is a more challenging approach to biomass particle combustion. CFD modeling is significantly more effective in terms of time and cost, in addition to being straightforward and safe to scale up. Consequently, this modeling can be adopted and referenced before conducting experimental studies. Concerning cocombustion, CFD analysis can elucidate the combustion results at all stages, including combustion characteristics, the

concentration of exhaust gas produced, and its performance (Yin et al., 2004).

This study utilized the ANSYS FLUENT software for CFD numerical simulation to analyze the co-combustion behavior and develop a 3D simulation model of a pulverized coal boiler. The primary fuel combustion process involved the utilization of LRC and additional OPF biomass as substitutes. The particle phase model's particle size ranges from a minimum diameter of 74-200 µm, with an average diameter of 134 µm (Bhuiyan & Naser, 2015). The reaction model employed for the combustion process utilizes the discrete ordinate (DO) radiation heat absorption technique. The absorptivity coefficient is calculated using the value of 0.6 obtained from the weighted sum of grey gases model (WSGGM) (Tabet & Gökalp, 2015). The k-E turbulence model is commonly employed to assess turbulent combustion flow in rotating systems (Westbrook & Dryer, 1981). P-1 solves radiation heat transfer by expanding the radiation intensity. The equations (1) to (3) represent the conservation of continuity, momentum, and total energy in the form of relevant equations.

Continuity Equation:

$$\frac{\partial_{\rho}}{\partial_{t}} + \nabla(\rho.\vec{v}) = S_{m} \tag{1}$$

Momentum Conservation:

$$\frac{\partial}{\partial_t}(\rho.\vec{v}) + \nabla \cdot (\rho.\vec{v}.\vec{v}) = -\nabla \rho + \nabla \cdot \vec{\tau} + \rho \cdot \vec{g} + \vec{F}$$
 (2)

Energy Conservation:

$$\frac{\partial}{\partial_t}(\rho.E) + \nabla[\vec{v}(\rho E + p)] = -\vec{v}(\sum_j h_j J_j) + S_h \tag{3}$$

This work employs continuity, momentum, and energy equations to simulate the co-firing process of biomass and coal within a combustion system. The continuity equation (1) ensures the mass balance of fuel and oxidant, whereas the momentum equation (2) delineates the dynamics of the combustion gas flow affected by pressure, viscosity, gravity, and additional external factors. The energy equation (3) incorporates the contributions of additional energy sources arising from the combustion reaction and heat transfer. The simulation encompasses several critical parameters: density (ρ), pressure (ρ), flow velocity (ν), viscosity (μ), and thermal conductivity (ν). The model integrates attributes of biomass and coal, including calorific value, mass fraction, and

combustion reaction rate. The initial conditions encompass the distribution of fuel, temperature, and gas composition within the combustion chamber. Boundary conditions are established according to the generator configuration, which includes inlet boundaries for air and fuel flows, output boundaries for combustion products, and wall conditions that account for heat transfer and radiation effects.

The study conducted proximate and ultimate analysis to determine the chemical contexture and enthalpy of generation of these components. Combining coal with oil palm fronds in a fire requires not one but two separate combustion processes. The model for coal combustion comprises two distinct phases: devolatilization and gas combustion. The references from sources (Adi Saputra *et al.*, 2024; Du *et al.*, 2017) adjust the kinetic rate parameters. Equations (4) to (7) express the coal combustion equation. The process of combusting *oil palm fronds* involves three specific stages: *drying, pyrolysis*, and *combustion*. The evidence for this combustion is presented in equations (8) to (10). Moreover, the kinetic rate characteristics of oil palm frond combustion serve as a standard for comparison (Aprianti *et al.*, 2023; Ihsan *et al.*, 2024).

Coal Combustion:

$$C_x H_y O_z N_w S_v + O_2 \to CO + H_2 O + N_2$$
 (4)

$$CO + 0.5O_2 \rightarrow CO_2 \tag{5}$$

$$CO + H_2O \rightarrow CO_2 + H_2 \tag{6}$$

$$H_2 + 0.5O_2 \to H_2O$$
 (7)

In the initial combustion reaction (equation 4), coal combines with oxygen to produce carbon monoxide (CO), water vapor H_2O , and nitrogen (N_2). The nitrogen and sulfur content of coal influences exhaust emissions such as NOx and SOx. Carbon monoxide oxidation (equation 5) occurs after early combustion, further oxidizing CO to carbon dioxide (CO_2). The water gas shift reaction (equation 6) involves CO combined with water vapor to form CO_2 and hydrogen (H_2), improving combustion efficiency. Oxygen oxide (Equation 7) indicates that the hydrogen produced in the previous reaction will react with oxygen to produce water vapor.

Oil Palm Frond Drying:

$$C_x H_y O_z N_w S_v + H_2 O (liquid) \rightarrow C_x H_y O_z N_w S_v + H_2 O (steam)$$
 (8)

Oil Palm Frond Pyrolysis:

$$C_x H_y O_z \to (C) + CO_2 + CH_4 \tag{9}$$

Oil Palm Frond Combustion:

$$C_x H_y O_z + O_2 \to C O_2 + H_2 O$$
 (10)

The evaporation of water content in biomass, as described in equation 8, refers to the drying process in which liquid water is converted into steam prior to combustion or pyrolysis. Pyrolysis of biomass (equation 9) occurs in a surrounding with no oxygen, resulting in the production of carbon (C), carbon dioxide (CO_2), and methane (CH_4). The resultant carbon may be utilized in subsequent combustion reactions. The combustion of biomass, as described in equation 10, represents the complete

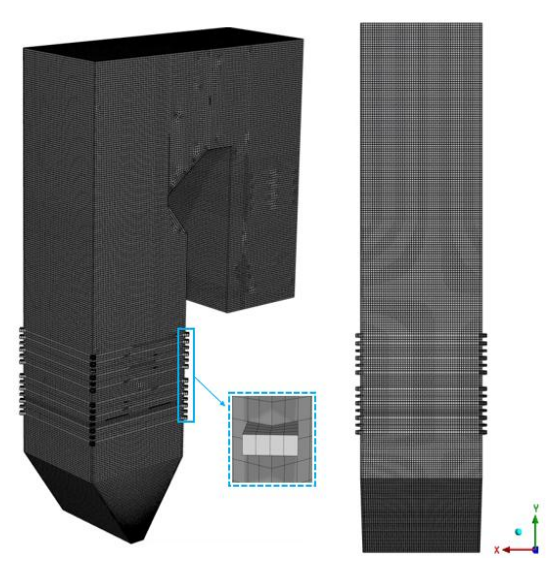


Fig. 4. Mesh-structured pulverized coal boiler

combustion process, yielding carbon dioxide and water vapor as the primary products.

This study models the combustion process through energy equations, momentum, and continuity to analyze the characteristics of chemical reactions, flow, and heat transfer involved. The principal reactions analyzed encompass coal combustion, pyrolysis, and biomass combustion, whilst the secondary reactions involve carbon monoxide oxidation and water-gas shift reactions. Simulations are performed by examining critical parameters, including fuel mix, reaction rate, temperature distribution, and combustion efficiency. The initial conditions are established according to the properties of the fuel and the combustion environment, whereas the boundary conditions encompass the air flow rate, fuel injection, and the release of combustion gases. The NOx modeling process occurs in a post-processing phase after the simulated combustion has been completed. This study also includes the development of modelling tools for NOx emissions, focusing on both thermal and fuel NOx models. Considering the negligible effect on NOx formation, the NO prompt model is omitted (Jiang et al., 2020; Yu et al., 2023).

4. Model Validation and Grid Independence

Three mesh models were examined in this work to address the complex pulverized coal domain: Meshing #A, Meshing #B, and 737.426 Meshing #C. The accuracy of the data results needs to be confirmed by additional independent investigation. Our goal is to make the grid domain very similar to real life as much as possible. The computational mesh domain for a pulverized coal boiler is depicted in Fig. 4. The PC boiler is rather complex; thus, it is important to simplify the model by separating it into its constituent parts. The meshing procedure in pre-processing for the simulation employs ANSYS FLUENT mesh software.

As shown in Table 5, three previously built grid network models were evaluated. Coarse, medium, and fine meshing (#A, #B, and #C, respectively) are related. Table 5's depiction of error deviations lends credence to this finding by confirming the pattern. Thus, meshing system #B is chosen for the simulation due to its ideal equilibrium between numerical precision and computational expenditure.

The temperature data gathered from the simulations by employing a flat plane positioned at 40 m height of a boiler, indicates that the mean surface temperature for all meshing data

Table 5Mesh quality of pulverized coal boiler on Meshing #2

| Quality Aspect | Minimum | Maximum | Average |
|--------------------|----------|---------|---------|
| Element Quality | 2.7e-003 | 1 | 0.89 |
| Aspect Ratio | 1 | 18 | 2.08 |
| Skewness | 1.4e-010 | 1 | 0.18 |
| Orthogonal Quality | 7 8e-008 | 1 | 0.88 |

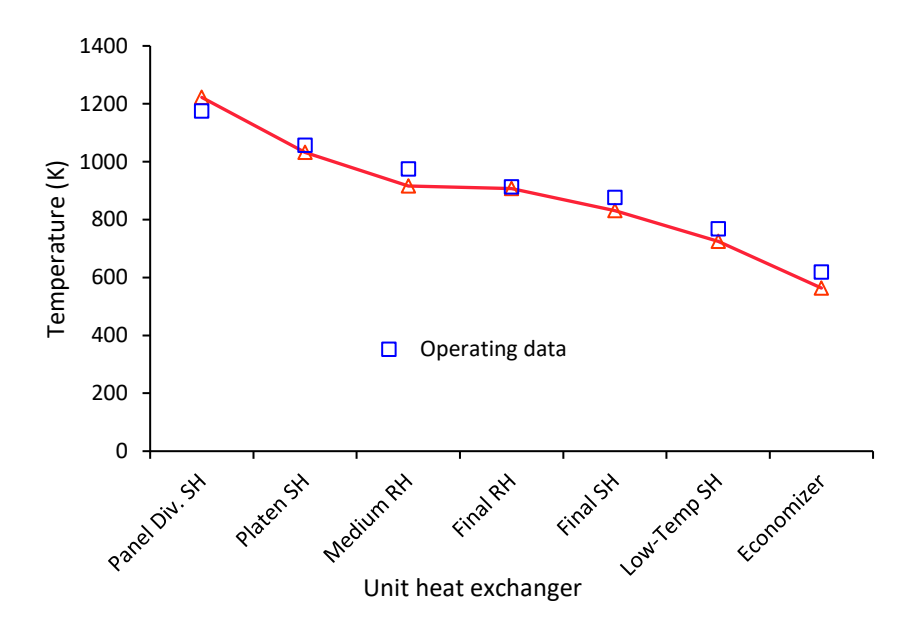


Fig. 5. Validation of operating data and simulation results (Ihsan et al., 2024)

#A is 1384.5 K, while meshing #B shows a value of 1306.1 K and meshing #C records a value of 1197.1 K. This investigation confirmed the exhaust gas temperature by comparing real data with simulated data to assess the accuracy of the simulation methodology. Further, the study validated the simulation approach by comparing it to the findings of previous research conducted by (Ihsan et al., 2024). Verification of the exhaust gas temperature between empirical data and simulated data is presented. The validation test was carried out utilizing these components, which are positioned on the tube bank of the heat exchanger in the Pacitan PLTU boiler. Figure 5 depicts the temperature distribution within the combustion cavity under biomass and coal co-firing conditions. The simulation curves are compared with the experimental data to assess the suitability of the model used. The graph demonstrates that the temperature distribution trend from the simulation closely matches the experimental data, especially in the primary combustion zone under actual boiler operating conditions at the pulverized coal FEGT design temperature of 1258.2 K.

5. Result and discussion

5.1. Temperature distribution

To achieve consistent combustion conditions, the difference in fuel characteristics between LRC coal and *oil palm frond* biomass must be burned in the boiler for an adequately long time. Introducing *oil palm frond* biomass as a fuel mixture from disparate inlet positions into the boiler room will undoubtedly impact the combustion characteristics. The combustion temperature in the boiler room serves as an indicator for

evaluating stable combustion conditions. To describe the temperature dispersion in the firing chamber, the middle position of the boiler has been selected for analysis in the cross-section simulation.

Figure 6 illustrates the simulated result of temperature distribution in the boiler's combustion chamber. It is a benchmark to compare with the co-firing case. Figure 6a, the temperature dispersion illustrates the peak location in the middle of the combustion chamber, where a symmetrical hot core exists. This profile highlights the vortex flow established by the tangential burner arrangement, into which fuel is injected from four corners (burners A-D), resulting in high turbulence in the central part of the chamber. It is a distribution showing a stable burning with a strong temperature of 1700 K confined within the principal combustion zones, i.e., the Lower Burning Zone (LBZ) and Upper Burning Zone (UBZ). The dominance of burners A and B characterizes the LBZ. The UBZ by burners C and D. This kind of even heat distribution enhances heat transfer efficiency to water pipes, which run along the chamber's walls. It enables the optimal generation of steam on the heat exhaust side FEGT (Bhuiyan et al., 2016a). Figure 6 presents the temperature profile and establishes a critical baseline for evaluating the performance of the co-firing system. This profile establishes a basis for assessing the alterations in temperature patterns resulting from the integration of OPF biomass into the burner. The temperature patterns that result from the integration of OPF biomass into the burner are assessed using this profile as a basis. This research investigates the impact of biomass on the stability of flames, heat transfer efficiency, and combustion behaviour within the combustion chamber (Demirbas, 2005).

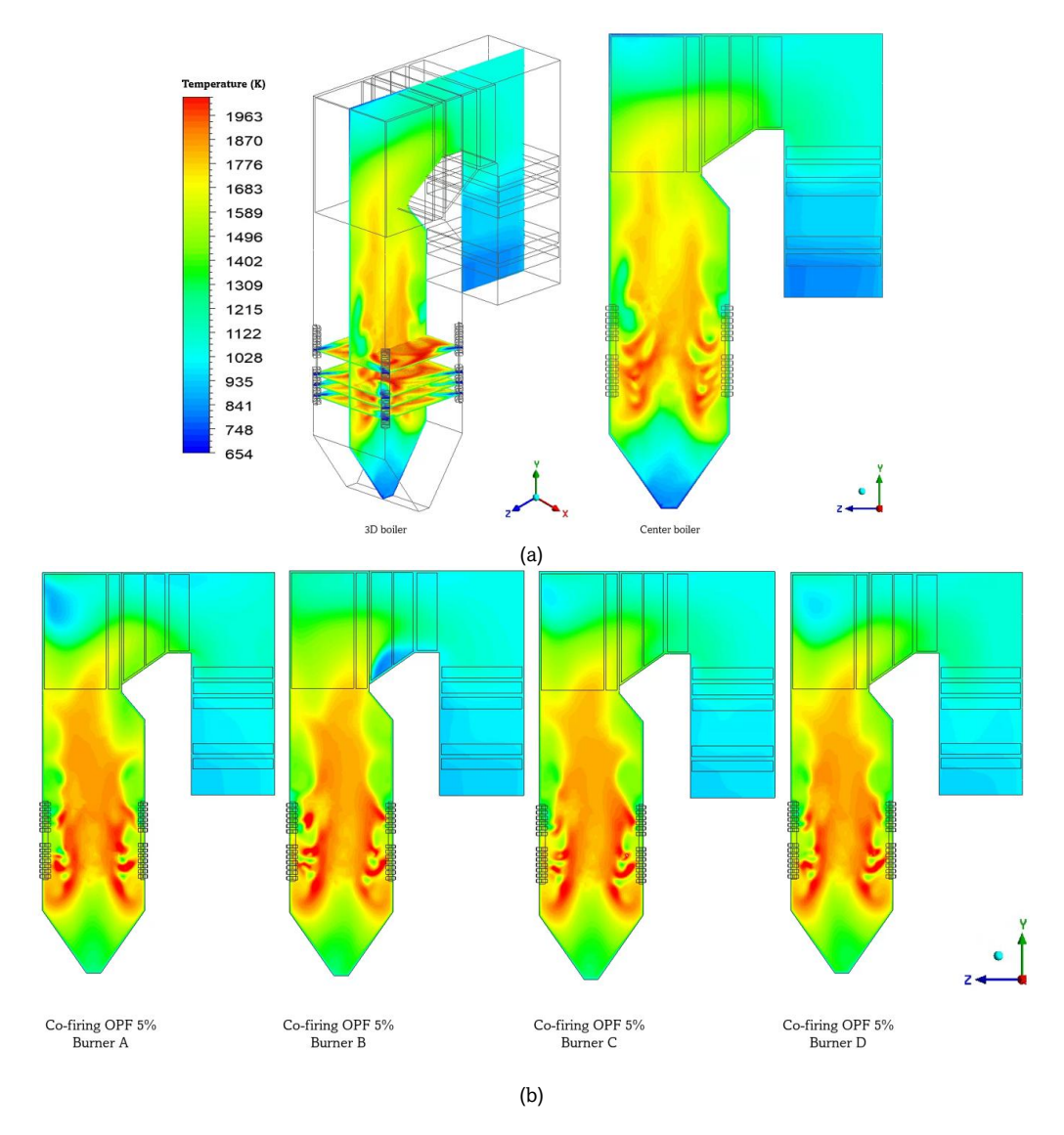


Fig. 6. Temperature distribution contours: (a) for full coal; (b) the boiler center for co-firing OPF 5% burners A-D

Figure 6b illustrates the temperature distribution within the combustion chamber during the co-firing of LRC coal, with 5% OPF injected into burners A to D. The temperature distribution pattern differs from that depicted in Figure 6. The hot spot points are in the middle region of the burning chamber; however, an appreciable increase in temperature exists in the top half of the UBZ. This finding means that the high oxygen content and volatility of OPF provide a more rapid release of energy and prolong the burning time in the upper part. The symmetrical temperature distribution enhances the stability of the flow vortex and maximizes heat transfer efficiency. The incorporation of OPF leads to increased temperatures following the primary combustion zone, especially in the Furnace Exit Gas Temperature (FEGT) and Overfire Air (OFA) areas, thus improving thermal efficiency (Ihsan *et al.*, 2024).

Figure 7 presents the temperature distribution. The Coffiring 5% OPF in burners A-D had minimal impact on combustion, except for a temperature increase in the upper furnace compared to full coal combustion. Fuel combustion occurs in the furnace's central region, which serves as the primary location of temperature distribution. Fuel inlets A and B form the Lower Burning Zone (LBZ), while fuel inlets C and D form the Upper Burning Zone (UBZ). These two parts divide the

combustion region. In the main region, close to the UBZ, you'll find the warmest temperatures. This increase shows that the fuel's combustion process starts as soon as it enters the combustion chamber through the intake. Combustion in tangential-type boilers must adhere to the critical boundary of creating a symmetrical temperature distribution ball. To the bottom of the LBZ, you'll find the bottom ash zone, where the ash particles that remain after combustion are sent. This area often has low temperatures when combustion is ideal. In real-world settings, it is common practice to release combustion gas emissions with a small amount of ash leftover particles.

Figure 7a presents the temperature profiles of all the burners (A-D) with coal alone as fuel. Burners A and B in the LBZ experience increased initial temperatures but a steep decline in the upper zone. Burners C and D in the UBZ experience a more stable temperature rise in the upper region. The data indicates that the UBZ burner maintains elevated temperatures over longer periods, which improves the thermodynamic efficiency of the boiler system, especially in the FEGT region (Bhuiyan *et al.*, 2016b). The distribution plays a vital role in assessing the impact of OPF addition on the performance of each burner zone, especially regarding high-temperature maintenance and flame stability in the upper zone of the combustion chamber.

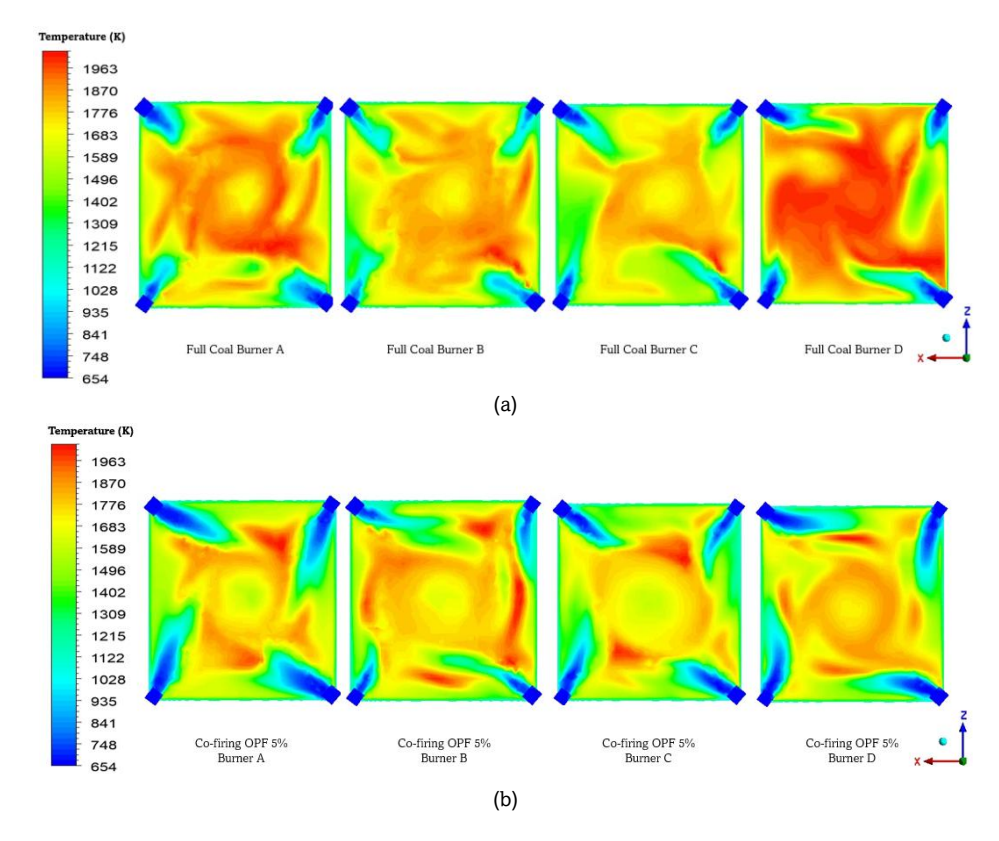


Fig. 7. Distribution of temperatures at each burner: (a) for full coal; (b) with co-firing OPF at 5% for burners A-D

Figure 7b represents the temperature profile of every burner (A-D) during 5% co-firing with OPF. The addition of OPF to burners A and B (LBZ) leads to a high rise in temperature at the first combustion zone; however, there is an abrupt drop in temperature at the middle to top zones. Adding OPF to burners C and D (UBZ) gives a higher temperature profile in the upper zone, with an extended temperature rise. The injection point of OPF significantly influences heat distribution and combustion efficiency. The C-D injection at the UBZ burner is revealed to be more efficient in providing higher temperature stability in the FEGT zone. The oxygen distribution of overfire air (OFA) plays a significant role in sustaining combustion in the upper zone (Yin et al., 2004).

This analysis was conducted using the injection tests for burners A to D across cases 1 to 4, all under conditions of complete coal combustion. The variation in temperature distribution within the furnace resulting from OPF injection across distinct burners (A-D) is affected by the positioning of the combustion zone. The injection of LBZ into burners A and B (LBZ) increases the release of heat in the initial combustion zone. However, the temperature in the upper middle section of the furnace decreases more rapidly. In contrast, the introduction of oxygen from the overfire air (OFA) results in a more uniform heat distribution in the upper zone, and the temperature elevation persists for a prolonged period, as a result of the injection in burners C and D (UBZ). The temperature stability and combustion efficiency are influenced by the distribution of oxygen within the combustion chamber.

The average temperature values were derived from the average area calculated during post-processing in ANSYS FLUENT. The lowest average temperature was observed in the bottom ash zone. At the same time, the main chamber of the pulverized coal boiler, situated at a height of 15-25 meters, recorded the highest average temperature of 1711.74 K.

Notably, co-firing with oil palm frond biomass resulted in a temperature reduction varying from 6.31% to 7.83% at this height. Conversely, after the afterburner procedure and the transition from the OFA zone to the FEGT zone, an increase in average temperature was noted, varying from 11.49% to 13.25% compared to conditions of full coal combustion. The reason for this is that the oxygen and volatile content in oil palm fronds surpass that of coal. The integration of OPF in co-combustion may affect flame stability and ignition delay due to differences in fuel properties compared to coal. OPF demonstrates a markedly elevated volatile percentage of 77.81%, whereas coal possesses a volatile value of roughly 33.76%. This indicates heightened flammability and a potential increase in the combustion rate within the boiler. This improves the initial combustion process, thereby contributing to flame stability. OPF exhibits a reduced fixed carbon content of 14.29% in contrast to coal's 32.31%, resulting in accelerated burnout and potential temperature variations within the boiler. Furthermore, the diminished moisture content of OPF at 5.81% compared to coal's 31.43% may result in a reduction of the energy required for initial drying, hence expediting the igniting process. The integration of OPF results in an increase in the average temperature in the upper furnace zone, hence improving combustion efficiency and ensuring boiler operational stability.

Figure 8 shows the average temperature distribution with height along the furnace for all cases of injection burners labeled as A-D. In Figure 8a from 15-25 meters of height, the main combustion zone has the highest temperature of approximately 1711.74 K. OPF co-firing reduces the average temperature in that zone by 6.31%-7.83% concerning coal combustion in the absence of any impurities. After going through the main combustion zone and entering the OFA to the FEGT region, the mean temperature increases between 11.49% and 13.25%. The increase can be attributed to the much greater volatile matter

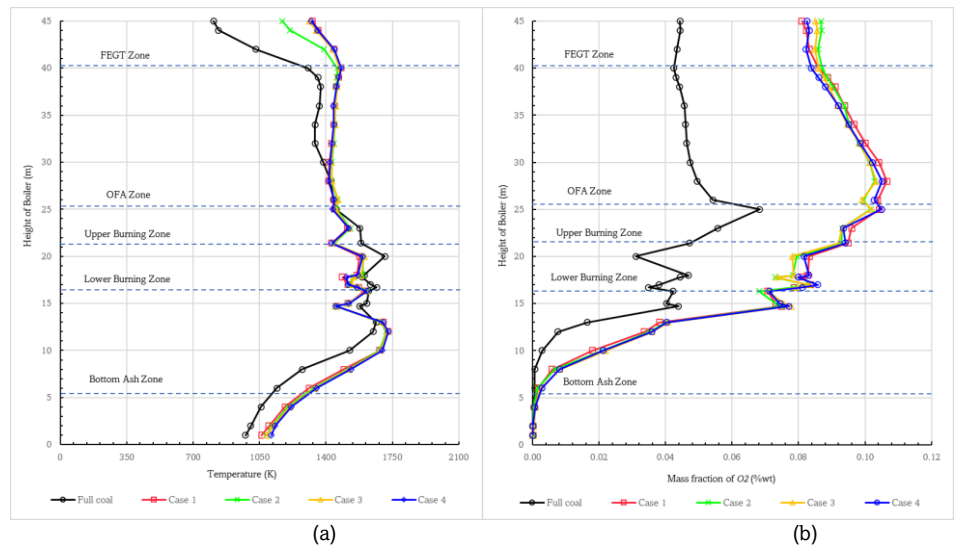


Fig. 8. Case simulation graph along the height of the furnace: (a) temperature distribution; (b) the O₂ distribution

content of Oil Palm Fronds (77.81%) compared to that of coal (33.76%), along with the higher oxygen content in Oil Palm Fronds that favors a more rapid energy release during secondary combustion after initial combustion (Jiang *et al.*, 2020; Tabet & Gökalp, 2015). The reduction of OPF moisture content to 5.81% enables faster drying and improved initial combustion efficiency. This trend implies that the co-firing methods must consider the point of injection and the primary zone of combustion to achieve the optimum thermal advantages of OPF biomass.

Figure 8b illustrates the oxygen (O_2) concentration distribution along the combustion chamber height in different OPF injection cases. In Case 1 of pure coal combustion, the O₂ content has a very steep decline in the primary combustion zone of 15-25 m, reflecting the peak oxygen consumption by the LRC combustion reaction. For co-firing 5% OPF in Cases 2-5, O, distribution shows a significant rise in the upper zone OFA-FEGT. This result is attributed to the higher oxygen content of OPF, at 41.66%, as opposed to 15.04% for LRC. Additionally, the volatile matter increase serves to accelerate and enhance the combustion reaction efficiency in the initial stage (Y. Wang & Yan, 2008). This result implies that OPF utilization improves the initial stages of combustion, thereby elevating the availability of free oxygen for secondary combustion and aiding emission control. As illustrated in Fig. 8, the efficiency of the combustion furnace generally increases with rising temperature. Nevertheless, the reduction in CO2 emissions from the cocombustion of LRC and palm oil fronds provides a compelling rationale for reducing reliance on fossil fuels, as illustrated in Fig. 10.

The result of the interaction between the oxygen-temperature distribution relationship in a boiler is the complex combustion process. In the combustion process, this interaction is a factor. The combustion process generates heat as a consequence of the oxygen consumption, which drives an increase in the temperatures of the lower and upper combustion zones. The OFA zone achieves optimal combustion and lower emissions by modulating temperature and enabling the introduction of oxygen. The data revealed that the co-firing scenario resulted in a more efficient combustion process compared to the scenario when coal was the exclusive fuel. The highly volatile component of biomass is responsible for increasing the rate of combustion and the amount of energy that is released. According to previous studies, the combination of

biomass with coal has the potential to increase thermal efficiency by anywhere from 5 to 10 percent, depending on the particular type of biomass that is utilized (Demirbas, 2005). Optimal blending can mitigate these negative impacts by adjusting the mixing ratio and selecting biomass types with lower alkali content. The use of additives like kaolin has been demonstrated to effectively mitigate the effects of fouling and slagging in coal-biomass-based boilers (Werther et al., 2000). The findings of this study align with previous research that indicated biomass co-firing influences boiler thermal efficiency, combustion variability, and temperature reduction. To mitigate the effects of biomass blending, additional studies have indicated that optimizing burner tuning and controlling the air ratio are essential. This study demonstrates that the successful implementation of co-firing in PLTU relies heavily on the application of effective operational techniques.

5.2 Distribution of CO2 and SO2 Emissions

Fig. 9 shows the distribution of CO_2 mass exhaust emissions. Essentially, the combustion of carbon in fossil fuels, particularly LRC coal, generates CO_2 mass. Higher gas concentration levels lead to enhanced combustion rate efficiency. In this instance, the combustion of LRC exhibits reduced efficiency at a particular altitude. The incomplete combustion of LRC coal can produce CO gas, which arises as a by-product of the carbon content and volatile substances present in the coal.

Figure 9a shows the contour of the CO2 mass fraction distribution in the combustion chamber during the full coal combustion process. The main combustion zone, including the LBZ and UBZ, is where the most intense combustion occurs as a result of the interaction between fuel and primary air. Consequently, the LBZ and UBZ contain the maximum concentration of CO_2 . The substantial increase in the CO_2 mass fraction in this zone suggests that the carbon is converted efficiently through perfect oxidation between carbon and oxygen to CO2. The vertical CO2 concentration decreases in the Furnace Exit Gas Temperature (FEGT) zone, indicating that most of the carbon in the coal has been converted to CO₂ before reaching the top of the combustion furnace. This condition shows the effectiveness of combustion in the tangential system. This phenomenon takes place when the fuel and air blend uniformly, facilitating the development of a balanced flame at the centre of the combustion furnace. The substantial carbon

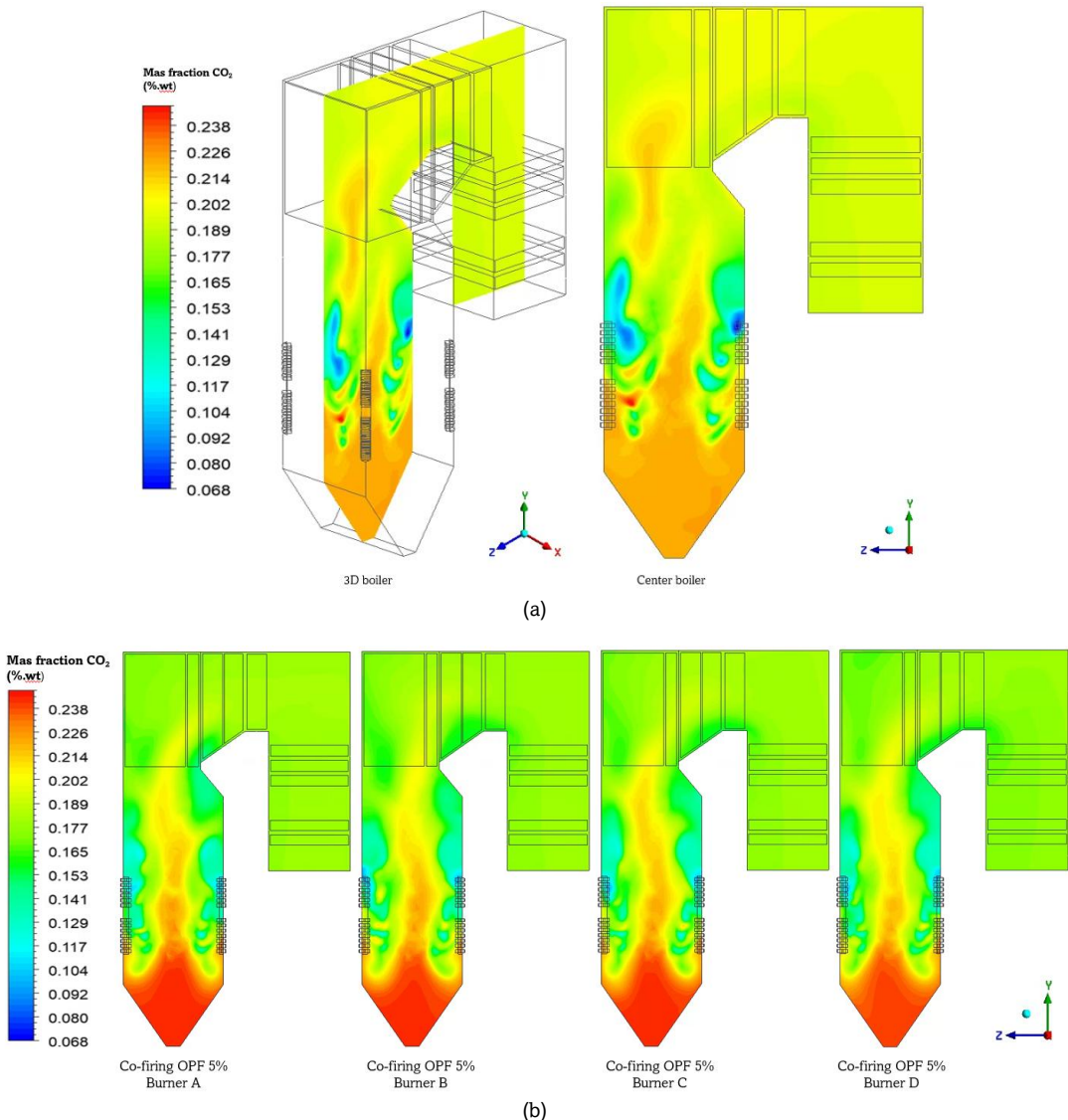


Fig. 9. CO, distribution contours: (a) for full coal; (b) boiler center for 5% OPF co-firing of burners A-D

content in coal, measured at 46.96%, plays a direct role in the significant CO₂ emissions produced. This finding demonstrates that burning pure coal without any biomass substitution leads to considerable greenhouse gas emissions. Consequently, this raises a concern in the initiatives aimed at shifting energy towards low-carbon emissions.

Figure 9b shows the variation of CO₂ distribution created by the co-firing operation with 5% OPF. A reduction in the concentration of CO₂ was apparent, especially in the upper zone, which is equivalent to a larger percentage of non-fossil biomass, which naturally emits less carbon. The reduction can be attributed to the lower carbon content of OPF at 44.37% compared to LRC at 46.96%. OPF is also a carbon-neutral fuel (Demirbas, 2005). The efficiency of carbon conversion during the rapid combustion of OPF helps reduce carbon monoxide formation as an intermediate product. The utilization of oil palm frond biomass in the co-combustion process has reduced CO₂ concentration within the upper region of the boiler furnace, since oil palm fronds do not possess carbon. This phenomenon is evident when the substitution of 5% at each injection of burners A to D results in a slight decrease in the CO2 mass fraction at each elevation. However, this is not significantly different from combustion using full LRC, which produces more

 CO_2 at most boiler heights, particularly in the combustion zone (as illustrated in Figs. 9). The highest SO_2 formation was observed in the LBZ and UBZ regions, with the SO_2 mass fraction reaching approximately 0.300 (%wt) in full LRC combustion. In contrast, co-combustion of 5% substitution oil palm fronds injected at burners A to D decreased the SO_2 mass fraction at each elevation, particularly in the OFA zone and further in the FEGT zone.

Figure 10 presents the graphs illustrating the mass distribution of CO_2 and SO_2 . Figure 10a presents the reduction trend of CO_2 mass fraction for all co-firing scenarios. 5% OPF substitution in burners A-D caused CO_2 reduction in the range of 27.96% to 31.18% relative to single coal combustion. The highest reduction was observed when OPF was injected in burner D (UBZ), indicating that the injection location affects carbon oxidation efficiency (Tabet & Gökalp, 2015). The distribution of CO_2 confirms the effectiveness of OPF in reducing carbon emissions through two primary mechanisms: lowering the carbon input from the fuel and improving carbon conversion efficiency during combustion. The effect of OPF addition on co-combustion results in better carbon conversion efficiency in the combustion process. This is due to the highly volatile matter and oxygen content in OPF, which increases the

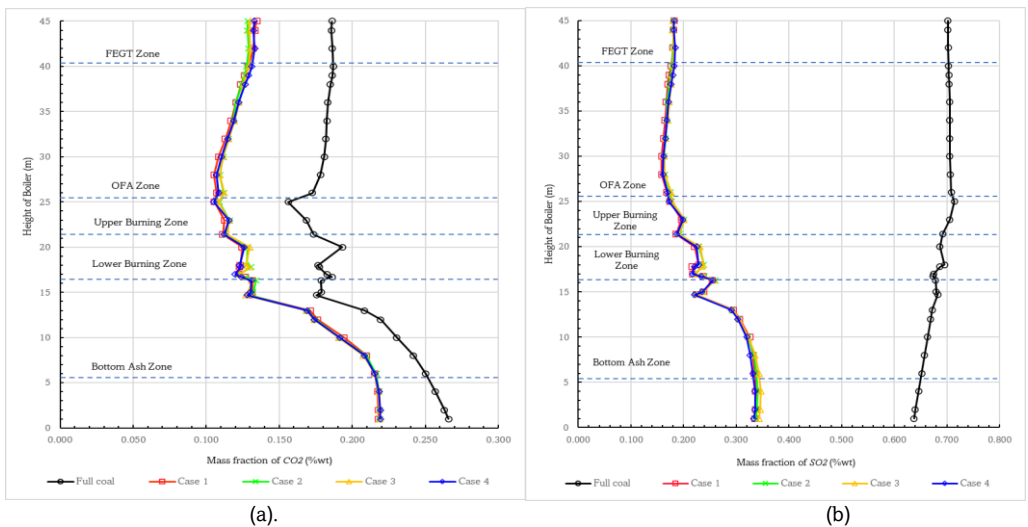


Fig. 10. Graph in each simulation case across the furnace height: (a) CO2 distribution; (b) SO2 distribution

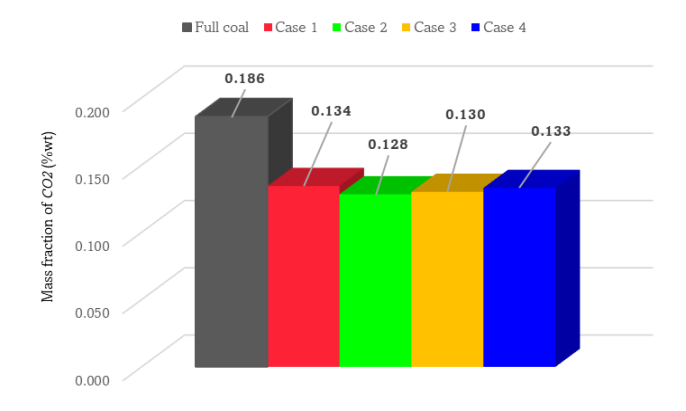


Fig. 11. Boiler outlet CO2 mass fraction comparison

combustion rate and optimizes the carbon oxidation process. Additionally, the carbon content in OPF is lower than that in coal, contributing to the reduction of CO2 emissions. The LBZ and UBZ are the areas where the most substantial decrease in CO2 emissions is observed. The primary site for intense combustion, particularly in the lower zone, is through injection in these two areas. This results in the early conversion of carbon into CO2, decreasing its concentration as fuel carbon is consumed. Regarding ash deposition concerns, OPF has a lower ash percentage of 2.09% compared to coal's 2.50%. This can diminish the occurrence of slagging and fouling in the boiler. The ash particles generated by OPF combust more readily before arriving at the heat exchanger. A minor fraction of the ash may still be transported with the exhaust gas, necessitating consideration in emission management and maintenance systems.

Figure 10b illustrates the downward trend of SO_2 mass fraction in all co-firing scenarios. During full coal combustion, the concentration of SO_2 was greatest at approximately 0.3% in both LBZ and UBZ zones, denoting the influence of the LRC sulfur content. OPF introduction brought about a gradual decline in the SO_2 content, more pronounced in the elevated OFA and FEGT concentrations. This result is because OPF has lower sulfur content, at 0.10%, as opposed to 0.12% in coal, and the sulfur volatility, making it more active in the gas phase. This

finding refers to the high potential of replacing some fossil fuels with low-sulfur biomass to reduce SO_2 emissions significantly.

The potential for utilizing palm frond waste biomass as a resource of clean energy in Indonesia is substantial, particularly when considering the support of infrastructure, technology, and government policies. Despite facing significant obstacles, such as costly operational and production expenses, adopting renewable energy sources derived from palm frond biomass represents a viable and appropriate solution for Indonesia's future energy needs. An additional benefit of incorporating palm frond biomass in co-burning processes is the reduction of carbon-containing fossil fuel usage. The findings of the comparison of simulated average CO2 mass fraction data at the furnace outlet are illustrated in Fig. 16. Co-firing effectively reduces exhaust emissions, particularly sulfur dioxide (SO2) and carbon dioxide (CO2). The low sulfur content in biomass facilitates the reduction of SO2, as demonstrated in a study by . The reduction of CO2 is significant as biomass is regarded as a carbon-neutral fuel, indicating that the CO2 emissions generated can be balanced by the CO₂ absorbed during biomass growth.

Figure 11 shows the comparative findings of the mean mass fraction of CO_2 at the boiler outlet for all the scenarios being studied. Surprisingly, all co-firing scenarios show a steady decrease in CO_2 emissions relative to pure coal combustion. The highest reduction in CO_2 emissions was recorded with the injection of OPF in burner B (LBZ) up to a whopping 31.18%.

This study affirms that the infusion of OPF in the upper zone enhances combustion efficiency and optimizes carbon conversion, all while minimizing excess emissions (Ihsan *et al.*, 2024). Furthermore, the OPF co-firing strategy effectively reduces carbon emissions and facilitates decarbonization by providing a low-emission alternative fuel approach.

5.3 Mass Fraction Distribution of NOx

The concentration of *NOx* demonstrates a notable increase in the primary furnace area (particularly in the BAZ region) during combustion, parallel to the injection of 5% *palm fronds* into each of burner A to D. The elevated combustion temperature gives a substantial rise to the formation of thermal *NOx* and fuel *NOx* mass fractions. Moreover, a reduction in *NOx* is observed in the LBZ, UBZ, and OFA regions. In this context, *NOx* concentrations will undergo chemical change into nitrogen.

Figure 12a illustrates the contour of NOx mass distribution during the entire coal combustion process. The elevated NOx mass fraction is concentrated in the lower furnace zone. Particularly in the BAZ and LBZ regions. In this region, thermal NOx generation primarily transpires when nitrogen combines with oxygen at elevated temperatures of approximately 1500 K. The presence of 0.66% organic nitrogen in coal leads to the creation of fuel NOx through the decomposition of nitrogen compounds during combustion devolatilization. In hotter areas,

this process makes it easier for NOx to settle (Du et al., 2017; Vassilev et al., 2013).

Under conditions of excess air and relatively low temperatures, the *NOx* content gradually decreases in the OFA and FEGT zones. This decrease signifies that a reduction response to *NO* has occurred, with the emission products being spread to the higher region due to the turbulent flow generated by the tangential burner configuration. The increase in *NOx* emissions from the combustion of pure coal constitutes a substantial environmental issue that requires resolution. Therefore, mitigation strategies such as flue gas recirculation, *low-NOx* burners, and air staging are crucial for sustaining optimal combustion efficiency and minimizing exhaust emissions.

Figure 12b shows the change of the NO_X distribution contour after 5% OPF addition in burners A-D. NO_X concentration rose in the primary combustion zone, i.e., in LBZ and UBZ zones. It was due to the organic nitrogen content of OPF (0.46%), albeit lower than coal's, which easily breaks down with high temperatures and forms a local peak of NO_X (Chae *et al.*, 2021). Nevertheless, following the primary combustion zone and reaching the OFA zone, the concentration of NO_X decreased. This reduction signifies the secondary reaction due to the heightened oxygen supply and the lowered temperature, which discourages the further formation of NO_X .

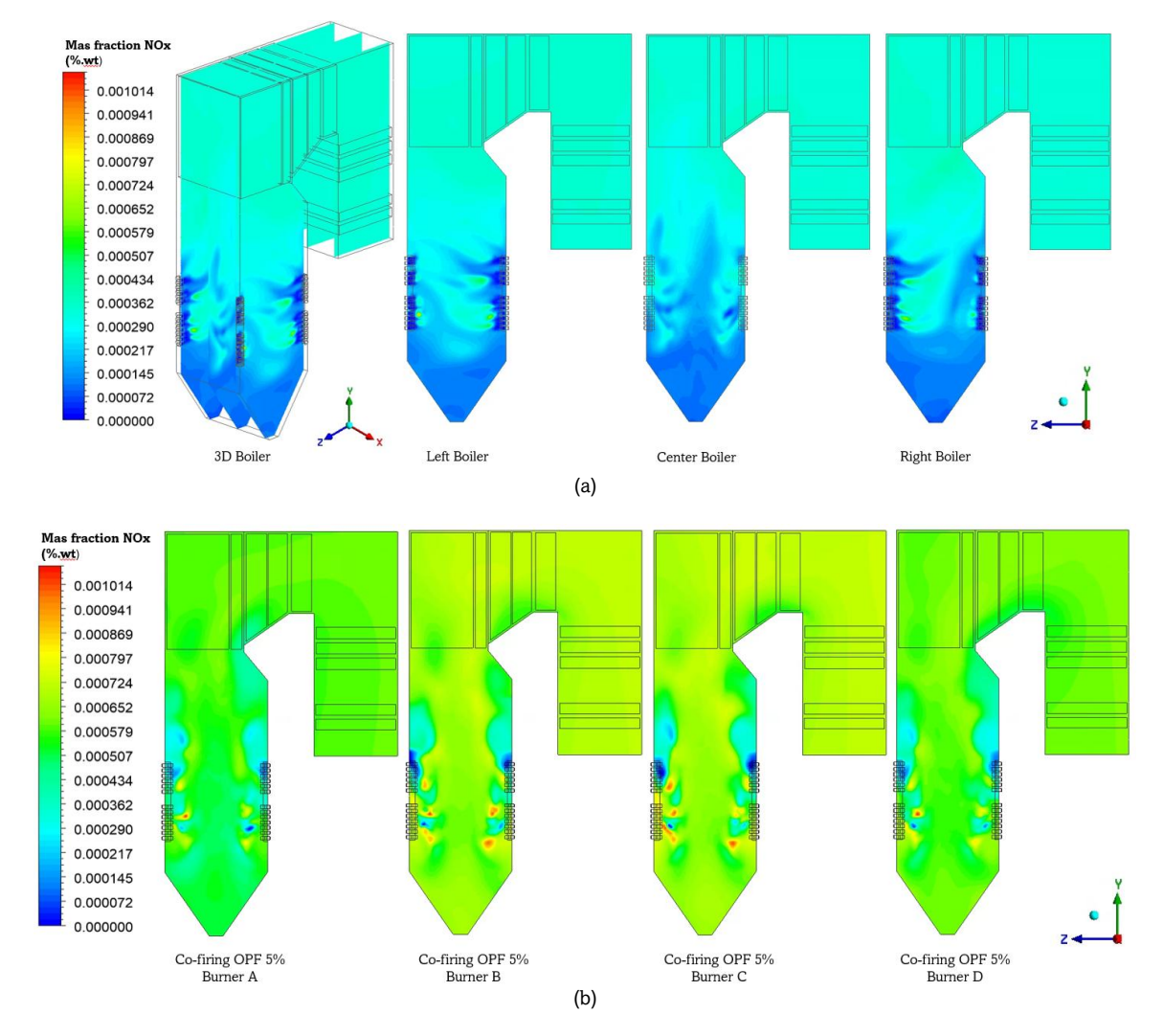


Fig. 12. Distribution contour of NOx mass fraction: (a) full coal; (b) boiler center for co-firing OPF 5% burner A-D (%wt)

This phenomenon may be attributed to the incineration of *palm fronds* in the primary zones of the furnace, namely the *Lower Burn Zone* (LBZ) and *Upper Burn Zone* (UBZ), which leads to a reduction in available *oxygen* in these regions. Consequently, this *oxygen* deficiency contributes to the incomplete combustion of coal-derived particles. The particles are primarily incinerated in the furnace's core section, which in turn results in a reduction of nitrogen compound emissions.

Figure 13 shows the vertical distribution of NO_x concentration for all cases. Co-firing with OPF produces a sharp rise in NO_x concentration of between 26.76% and 32.27% compared to burning with pure coal. The highest increase is observed after adding OPF to burner D (UBZ), possibly due to the higher temperature in the top zone and the more intense thermal- NO_x formation reaction. This graph indicates that OPF injection into the lower zone (burners A and B) results in a lower NO_x profile than the upper zone, as oxygen is absorbed more rapidly in the initial zone, inhibiting NO_x generation in the upper region. NOx concentration increases due to organic nitrogen in palm frond biomass, which decomposes during hightemperature combustion processes. As illustrated in Fig. 14, there is a corresponding rise in NOx emissions across specific simulations. When 5% of palm fronds are burned in burners A through D, the average increase in NOx emissions is recorded at 29.41% compared to complete coal combustion. Case 1 demonstrates a 32.27% increase, Case 2 exhibits a 26.76% increase, Case 3 reflects a 28.27% increase, and Case 4 indicates a 30.34% increase. Increased NOx emissions may lead to the formation of tropospheric ozone (O₃) via reactions with volatile organic compounds under sunlight, potentially harming human health. Additionally, the reaction of NOx with water, oxygen, and other atmospheric compounds can elevate acidity levels, potentially harming the environment. NO_x emissions are influenced by variations in temperature and the excess air ratio. High-temperature combustion can elevate thermal NO_x levels, whereas optimizing air distribution may mitigate its formation (Vassilev et al., 2013). Multiple mitigation measures may be applied in this context. Examples include staged combustion via air ratio regulation in various combustion zones, flue gas recirculation by reintroducing a portion of the flue gas into the combustion chamber, and selective non-catalytic reduction (SNCR) techniques that involve ammonia injection into the

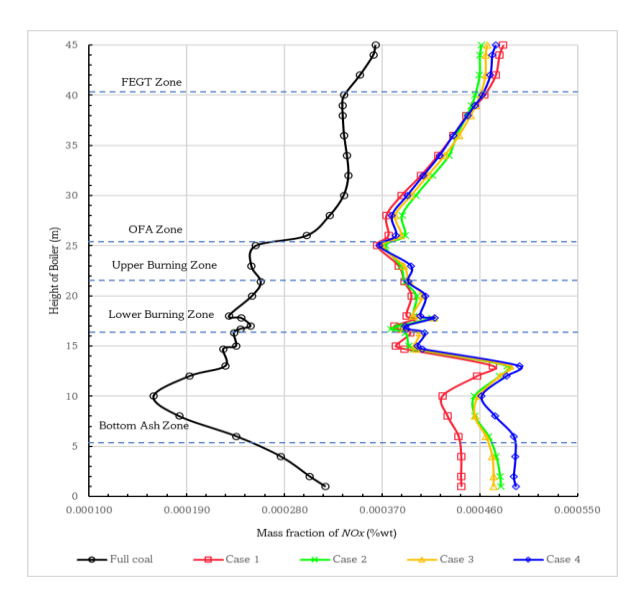


Fig. 13. *NOx* distribution graph in each simulation case across the furnace height

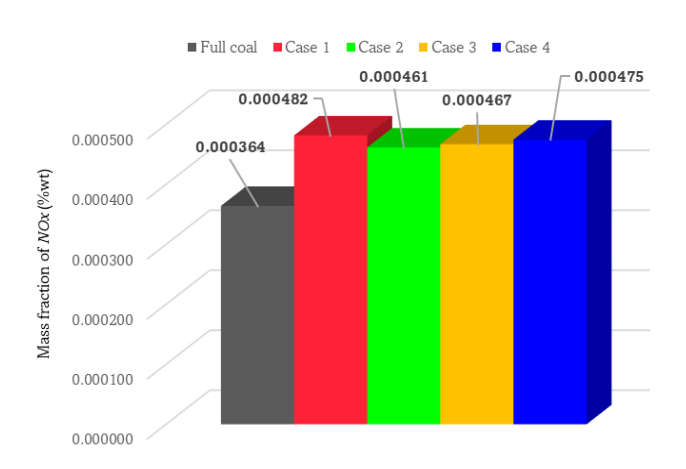


Fig 14. Boiler outlet NOx mass fraction comparison

combustion chamber at designated temperatures. (Adi Saputra et al., 2024).

Furthermore, a more efficient approach is the use of *low-NOx burners* (LNR), which achieve reduced temperature combustion by slowing the mixing of air and fuel. Implementing this strategy can mitigate the adverse effects of rising *NOx* emissions while maintaining combustion efficiency. Therefore, in order to determine the best approach for the biomass cofiring PLTU boiler system, additional research is necessary. Operating and maintenance costs for power plants that co-fire oil palm fronds with coal are far higher than those for units that burn coal alone. While incorporating oil palm frond biomass in co-firing has the potential to significantly reduce CO_2 and SO_2 *emissions*, it is accompanied by a substantial decrease in gross income. Therefore, utilizing pure coal remains a financially viable alternative under current conditions.

Figure 14 presents a comparison of the NO_x mass fraction at the boiler outflow under all conditions. Co-firing with OPF leads to an average increase of 29.41% in NO_x emissions at the output. The highest growth was recorded in OPF injection at burner D (32.27%), while the lowest was noted at burner A (26.76%). The rise in emissions is a serious setback in biomass co-firing and, therefore, requires careful balancing with other mitigation strategies such as staged combustion, recirculating flue gas (RFG), and selective non-catalytic reduction (SNCR). Further, the use of low- NO_x burners and modifying the secondary air-to-air ratio can also reduce NO_x formation without compromising combustion efficiency.

6. Conclusion

This study assesses the co-firing of coal with 5% oil palm fronds at different burner levels using computational techniques. Co-firing with 5% palm fronds raises the combustion temperature compared to exclusive coal combustion. The highly volatile content of palm fronds enhances heat transfer beyond the combustion chamber. The observed temperature increase is supported by measurements in the FEGTs area, indicating a possible improvement in combustion energy efficiency. The simulation model indicates that using 5% palm fronds in coalburning leads to a reduction in $\rm CO_2$ emissions ranging from 27.96% to 31.18%, as compared to total coal combustion. Significant reductions are noted in the LBZ and UBZ zones, indicating the efficacy of co-firing in reducing carbon emissions.

The findings of this study indicate that oil palm fronds could potentially function as a feasible alternative fuel in coal combustion systems utilized in boilers. The stability of combustion temperature indicates its potential applicability. Further research is necessary to optimize the NO_x emission reduction methods and assess their impact on overall carbon emissions. Subsequent research will investigate co-firing with medium-rank coal (MRC), oil palm fronds, and oil palm empty fruit bunches to expand the alternatives for sustainable fuels.

Abbreviations

| EFB | Empty Fruit Bunch |
|-----|------------------------------|
| OPF | Oil Palm Frond |
| PKS | Plam Kernel Shell |
| HT | Hydrothermal |
| CFD | Computational Fluid Dynamics |

PC Pulverized Coal OFA Overfire Air

FEGT Furnace Exit Gas Temperature

LRC Low-Rank Coal
PA Primary Air
SA Secondary Air
DO Discrete Ordinate

WSGGM Weighted Sum Grey Gases Model

LBZ Lower Burning Zone
UBZ Upper Burning Zone
BAZ Bottom Ash Zone
RH Reheater
SH Superheater

Chemical Symbol

| C | Carbon |
|----|------------|
| Н | Hydrogen |
| 0 | Oxygen |
| N | Nitrogen |
| S | Sulfur |
| NO | Nitrogon C |

 $\begin{array}{lll} \text{NO}_{\text{x}} & \text{Nitrogen Oxide} \\ \text{CO} & \text{Carbon Monoxide} \\ \text{CO}_{\text{2}} & \text{Carbon Dioxide} \end{array}$

H₂O Water

Acknowledgments

The authors gratefully acknowledge the financial assistance provided by the Indonesian Education Scholarship (BPI), the Higher Education Financing and Assessment Center (PPAPT), and Indonesia's Endowment Fund for Education (LPDP), as well as the experts who contributed valuable ideas to enhance the quality and substance of this research.

References

- Adi Saputra, I. N. A., Manurung, T. D., Yuliadi, A. E., Prabowo, Nugroho, G., Kusumadewi, T. V., Hariana, H., & Chan, S. H. (2024). Numerical simulation of co-firing LRC and ammonia in Pangkalan Susu 3 & 4 coal-fired steam power plant (CFSPP) capacity 210 megawatts. Case Studies in Thermal Engineering, 63. https://doi.org/10.1016/j.csite.2024.105230
- Agus Adi Saputra, I. N., Prabowo, Setiyawan, A., Bagus Wijaya Kusuma, I. G., Ihsan, S., & Darmawan, A. (2024). Numerical Simulation Co-Firing Of EFB And LRC Injected At Different Burner Levels In Tangential Combustion-Type Pulverized Boilers. 2024 10th International Conference on Smart Computing and Communication, ICSCC 2024, 328–332. https://doi.org/10.1109/ICSCC62041.2024.10690373
- Agus Adi Saputra, I. N., Prabowo, Setiyawan, A., Bagus Wijaya Kusuma, I. G., Ihsan, S., & Hariana. (2023). 3D Simulation Combustion Characteristics Of EFB Biomass Co-Firing With Low Rank Coal In Pulverized Coal Boiler. 2023 International Conference on Advanced Mechatronics, Intelligent Manufacture and Industrial

- Automation, ICAMIMIA 2023 Proceedings, 370–374. https://doi.org/10.1109/ICAMIMIA60881.2023.10427894
- Aprianti, N., Kismanto, A., Supriatna, N. K., Yarsono, S., Nainggolan, L. M. T., Purawiardi, R. I., Fariza, O., Ermada, F. J., Zuldian, P., Raksodewanto, A. A., & Alamsyah, R. (2023). Prospect and challenges of producing carbon black from oil palm biomass: A review. In *Bioresource Technology Reports* (Vol. 23). Elsevier Ltd. https://doi.org/10.1016/j.biteb.2023.101587
- Arifin, Z., Insani, V. F. S., Idris, M., Hadiyati, K. R., Anugia, Z., & Irianto, D. (2023). Techno-Economic Analysis of Co-Firing for Pulverized Coal Boilers Power Plant in Indonesia. *International Journal of Renewable Energy Development*, 12(2), 261–269. https://doi.org/10.14710/ijred.2023.48102
- Aziz, M., Budianto, D., & Oda, T. (2016). Computational fluid dynamic analysis of co-firing of palm kernel shell and coal. *Energies*, 9(3). https://doi.org/10.3390/en9030137
- Aziz, M., Oda, T., & Kashiwagi, T. (2015). Innovative Steam Drying of Empty Fruit Bunch with High Energy Efficiency. *Drying Technology*, 33(4), 395–405. https://doi.org/10.1080/07373937.2014.970257
- Aziz, M., Prawisudha, P., Prabowo, B., & Budiman, B. A. (2015). Integration of energy-efficient empty fruit bunch drying with gasification/combined cycle systems. *Applied Energy*, 139, 188– 195. https://doi.org/10.1016/j.apenergy.2014.11.038
- Bhuiyan, A. A., Karim, M. R., & Naser, J. (2016a). Modeling of Solid and Bio-Fuel Combustion Technologies. In *Thermofluid Modeling for Energy Efficiency Applications* (pp. 259–309). Elsevier Inc. https://doi.org/10.1016/B978-0-12-802397-6.00016-6
- Bhuiyan, A. A., Karim, M. R., & Naser, J. (2016b). Modeling of Solid and Bio-Fuel Combustion Technologies. In *Thermofluid Modeling for Energy Efficiency Applications* (pp. 259–309). Elsevier Inc. https://doi.org/10.1016/B978-0-12-802397-6.00016-6
- Bhuiyan, A. A., & Naser, J. (2015). Computational modelling of co-firing of biomass with coal under oxy-fuel condition in a small scale furnace. *Fuel*, *143*, 455–466. https://doi.org/10.1016/j.fuel.2014.11.089
- Cahyo, N., Sulistiyowati, D., Rahmanta, M. A., Felani, M. I., Soleh, M., Paryanto, P., Prismantoko, A., & Hariana, H. (2024). A technoeconomic and environmental analysis of co-firing implementation using coal and wood bark blend at circulating fluidized bed boiler. *International Journal of Renewable Energy Development, 13*(4), 726–735. https://doi.org/10.61435/IJRED.2024.60234
- Chae, T., Lee, J., Lee, Y., Yang, W., & Ryu, C. (2021). Pilot-scale experimental study on impacts of biomass cofiring methods to nox emission from pulverized coal boilers—part 2: Nox reduction capability through reburning versus cofiring. *Energies*, *14*(20). https://doi.org/10.3390/en14206552
- Chiaramonti, D., Prussi, M., Buffi, M., Rizzo, A. M., & Pari, L. (2017). Review and experimental study on pyrolysis and hydrothermal liquefaction of microalgae for biofuel production. *Applied Energy*, *185*, 963–972. https://doi.org/10.1016/j.apenergy.2015.12.001
- Darmawan, A., Budianto, D., Aziz, M., & Tokimatsu, K. (2017).

 Retrofitting existing coal power plants through cofiring with hydrothermally treated empty fruit bunch and a novel integrated system. *Applied Energy*, 204, 1138–1147. https://doi.org/10.1016/j.apenergy.2017.03.122
- Demirbas, A. (2005). Potential applications of renewable energy sources, biomass combustion problems in boiler power systems and combustion related environmental issues. *Progress in Energy and Combustion Science*, 31(2), 171–192. https://doi.org/10.1016/j.pecs.2005.02.002
- Du, Y., Wang, C., Lv, Q., Li, D., Liu, H., & Che, D. (2017). CFD investigation on combustion and NOx emission characteristics in a 600 MW wall-fired boiler under high temperature and strong reducing atmosphere. *Applied Thermal Engineering*, 126, 407–418. https://doi.org/10.1016/j.applthermaleng.2017.07.147
- Garcia-Nunez, J. A., Ramirez-Contreras, N. E., Rodriguez, D. T., Silva-Lora, E., Frear, C. S., Stockle, C., & Garcia-Perez, M. (2016). Evolution of palm oil mills into bio-refineries: Literature review on current and potential uses of residual biomass and effluents. In Resources, Conservation and Recycling, 110(99–114). https://doi.org/10.1016/j.resconrec.2016.03.022
- Ghosh, A., Brown, J. L., Smith, R. G., & Brown, R. C. (2023). Hydrolysis of anhydrosugars derived from pyrolysis of lignocellulosic

- biomass for integration in a biorefinery. Sustainable Energy and Fuels, 7(14), 3361–3374. https://doi.org/10.1039/d3se00240c
- Hariana, H., Putra, H. P., Prabowo, Hilmawan, E., Darmawan, A., Mochida, K., & Aziz, M. (2023a). Theoretical and Experimental Investigation of Ash-Related Problems During Coal Co-Firing With Different Types of Biomass in a Pulverized Coal-Fired Boiler. Energy, 269, 126784. https://doi.org/10.1016/j.energy.2023.126784
- Hariana, H., Putra, H. P., Prabowo, Hilmawan, E., Darmawan, A., Mochida, K., & Aziz, M. (2023b). Theoretical and Experimental Investigation of Ash-Related Problems During Coal Co-Firing With Different Types of Biomass in a Pulverized Coal-Fired Boiler. *Energy*, 269, 126784. https://doi.org/10.1016/j.energy.2023.126784
- Ibbett, R., Gaddipati, S., Davies, S., Hill, S., & Tucker, G. (2011). The mechanisms of hydrothermal deconstruction of lignocellulose: New insights from thermal-analytical and complementary studies. Bioresource Technology, 102(19), 9272–9278. https://doi.org/10.1016/j.biortech.2011.06.044
- Ihsan, S., Prabowo, Widodo, W. A., & Adi Saputra, I. N. A. (2023). Numerical Investigation Effect of the addition of palm fronds on the burning of coal-fired boilers tangentially. 2023 International Conference on Advanced Mechatronics, Intelligent Manufacture and Industrial Automation, ICAMIMIA 2023 - Proceedings, 261–265. https://doi.org/10.1109/ICAMIMIA60881.2023.10427970
- Ihsan, S., Prabowo, Widodo, W. A., Saputra, I. N. A. A., & Hariana. (2024).

 Utilization of Palm Frond Waste as Fuel for Co-Firing Coal and Biomass in a Tangentially Pulverized Coal Boiler Using Computational Fluid Dynamic Analysis. *Biomass*, 4(4), 1142–1163. https://doi.org/10.3390/biomass4040063
- Jamari, S. S., & Howse, J. R. (2012). The effect of the hydrothermal carbonization process on palm oil empty fruit bunch. *Biomass and Bioenergy*, 47, 82–90. https://doi.org/10.1016/j.biombioe.2012.09.061
- Jiang, Y., Park, K. H., & Jeon, C. H. (2020). Feasibility study of co-firing of torrefied empty fruit bunch and coal through boiler simulation. *Energies*, 13(12). https://doi.org/10.3390/en13123051
- Kim, S., Kim, H. J., & Park, J. C. (2009). Application of recycled paper sludge and biomass materials in manufacture of green composite pallet. *Resources, Conservation and Recycling*, 53(12), 674–679. https://doi.org/10.1016/j.resconrec.2009.04.021
- Kumar, K., Tyagi, U., Sirohi, S., Kumar, R., Kumar Maity, S., Nikita, Singh, S., & Kumar, G. (2025). A critical review on nanostructure-doped carbonized biomass: A new Era in sustainable supercapacitor technology. In *Fuel* (Vol. 381). Elsevier Ltd. https://doi.org/10.1016/j.fuel.2024.133707
- Lam, P. S., Lam, P. Y., Sokhansanj, S., Lim, C. J., Bi, X. T., Stephen, J. D., Pribowo, A., & Mabee, W. E. (2015). Steam explosion of oil palm residues for the production of durable pellets. *Applied Energy*, 141, 160–166. https://doi.org/10.1016/j.apenergy.2014.12.029
- Li, W., Guo, J., Cheng, H., Wang, W., & Dong, R. (2017). Two-phase anaerobic digestion of municipal solid wastes enhanced by hydrothermal pretreatment: Viability, performance and microbial community evaluation. *Applied Energy*, 189, 613–622. https://doi.org/10.1016/j.apenergy.2016.12.101
- Liu, Z., Quek, A., Kent Hoekman, S., & Balasubramanian, R. (2013). Production of solid biochar fuel from waste biomass by hydrothermal carbonization. *Fuel*, 103, 943–949. https://doi.org/10.1016/j.fuel.2012.07.069
- Lucian, M., & Fiori, L. (2017). Hydrothermal carbonization of waste biomass: Process design, modeling, energy efficiency and cost analysis. *Energies*, 10(2). https://doi.org/10.3390/en10020211
- Putra, H. P., Kuswa, F. M., Prabowo, & Hariana, H. (2023). Utilization of Calliandra Calothyrsus and Gliricidia Sepium as Co-Firing Fuel

- With Consideration of Ash-Related Issues. *Iop Conference Series Earth and Environmental Science*, 1281(1), 12014. https://doi.org/10.1088/1755-1315/1281/1/012014
- Rahman, M. N., Yusup, S., Chin, B. L. F., Shariff, I., & Quitain, A. T. (2023).

 Oil Palm Wastes Co-Firing in an Opposed Firing 500 MW Utility
 Boiler: A Numerical Analysis. *CFD Letters*, *15*(3), 139–152.

 https://doi.org/10.37934/cfdl.15.3.139152
- Román, S., Nabais, J. M. V., Laginhas, C., Ledesma, B., & González, J. F. (2012). Hydrothermal carbonization as an effective way of densifying the energy content of biomass. *Fuel Processing Technology*, 103, 78–83. https://doi.org/10.1016/j.fuproc.2011.11.009
- Su, X., Chen, X., Fang, Q., Ma, L., Tan, P., Zhang, C., Chen, G., & Yin, C. (2024). An integrated model for flexible simulation of biomass combustion in a travelling grate-fired boiler. *Energy*, 307. https://doi.org/10.1016/j.energy.2024.132605
- Tabet, F., & Gökalp, I. (2015). Review on CFD based models for co-firing coal and biomass. In *Renewable and Sustainable Energy Reviews* (Vol. 51, pp. 1101–1114). Elsevier Ltd. https://doi.org/10.1016/j.rser.2015.07.045
- Tirumareddy, P., Patra, B. R., Borugadda, V. B., & Dalai, A. K. (2024). Cohydrothermal liquefaction of waste biomass: Comparison of various feedstocks and process optimization. *Bioresource Technology Reports*, 27. https://doi.org/10.1016/j.biteb.2024.101898
- Torres Ramos, R., Valdez Salas, B., Montero Alpírez, G., Coronado Ortega, M. A., Curiel Álvarez, M. A., Tzintzun Camacho, O., & Beleño Cabarcas, M. T. (2023). Torrefaction under Different Reaction Atmospheres to Improve the Fuel Properties of Wheat Straw. *Processes*, 11(7). https://doi.org/10.3390/pr11071971
- Usino, D. O., Sar, T., Ylitervo, P., & Richards, T. (2023). Effect of Acid Pretreatment on the Primary Products of Biomass Fast Pyrolysis. *Energies*, 16(5). https://doi.org/10.3390/en16052377
- Vassilev, S. V., Baxter, D., Andersen, L. K., & Vassileva, C. G. (2013). An overview of the composition and application of biomass ash. Part
 1. Phase-mineral and chemical composition and classification.
 Fuel, 105, 40–76. https://doi.org/10.1016/j.fuel.2012.09.041
- Wang, Y., & Yan, L. (2008). CFD studies on biomass thermochemical conversion. *International Journal of Molecular Sciences*, 9(6), 1108–1130. https://doi.org/10.3390/ijms9061108
- Wang, Z., Yu, D., Han, J., & Wu, J. (2021). Impacts of Torrefaction on PM10 Emissions from Biomass Combustion. *Energy Engineering*, 118(5), 1267–1276. https://doi.org/10.32604/ee.2021.016107
- Werther, J., Saenger, M., Hartge, E. U., Ogada, T., & Siagi, Z. (2000). Combustion of agricultural residues. *Progress in Energy and Combustion Science*, 26(1), 1–27. https://doi.org/10.1016/S0360-1285(99)00005-2
- Westbrook, C. K., & Dryer, F. L. (1981). Simplified Reaction Mechanisms for the Oxidation of Hydrocarbon Fuels in Flames. *Combustion Science and Technology*, 27(1–2), 31–43. https://doi.org/10.1080/00102208108946970
- Wongsiriwittaya, M., Chompookham, T., & Bubphachot, B. (2023). Improvement of Higher Heating Value and Hygroscopicity Reduction of Torrefied Rice Husk by Torrefaction and Circulating Gas in the System. *Sustainability (Switzerland)*, 15(14). https://doi.org/10.3390/su151411193
- Yin, C., Rosendahl, L., Kær, S. K., & Condra, T. J. (2004). Use of numerical modeling in design for co-firing biomass in wall-fired burners. *Chemical Engineering Science*, 59(16), 3281–3292. https://doi.org/10.1016/j.ces.2004.04.036
- Yu, Y., Xu, L., Zhu, G., Liu, Y., & Niu, Y. (2023). Synergistical reduction of PM and NO formation in preheating co-firing of coal and biomass. *Journal of Cleaner Production*, 425. https://doi.org/10.1016/j.jclepro.2023.138918



© 2025. The Author(s). This article is an open-access article distributed under the terms and conditions of the Creative Commons Attribution-ShareAlike 4.0 (CC BY-SA) International License (http://creativecommons.org/licenses/by-sa/4.0/)